DOI:
10.1002/adma.202406611

Document Version
Peer reviewed version

Citation for published version (APA):
Yang, Y., Read, H., Sbai, M., Zareei, A., Forte, A. E., Melancon, D., & Bertoldi, K. (2024). Complex Deformation in Soft Cylindrical Structures via Programmable Sequential Instabilities. *Advanced Materials*, *36*(46), Article 2406611. https://doi.org/10.1002/adma.202406611

Complex deformation in soft cylindrical structures via programmable sequential instabilities

Yi Yang[a,*], **Helen Read**[a,*], **Mohammed Sbai**[a], **Ahmad Zareei**[a], **Antonio Elia Forte**[a,b], **David Melancon**[a,c,†], **and Katia Bertoldi**[a,†]

[a]J.A. Paulson School of Engineering and Applied Sciences, Harvard University, Cambridge, MA 02138, USA; [b]Department of Engineering, Kings College London, London, WC2R 2LS, UK; [c]Department of Mechanical Engineering, Polytechnique Montreal, Quebec, H3T 1J4, Canada; [*]These authors contributed equally

The substantial deformation exhibited by hyperelastic cylindrical shells under pressurization makes them an ideal platform for programmable inflatable structures. If we instead apply negative pressure, the cylindrical shell will buckle, leading to a sequence of rich deformation modes, all of which are fully recoverable due to the hyperelastic material choice. While the initial buckling event under vacuum is well understood, here, we explore the post-buckling regime and identify a region in the design space in which a coupled twisting-contraction deformation mode occurs; by carefully controlling the geometry of our homogeneous shells, we can control the proportion of contraction vs. twist. Additionally, we can unlock bending as a post-buckling deformation mode by varying the thickness of our shells across the circumference. Since these soft shells can fully recover from the substantial deformations caused by buckling, we then harness these instability-driven deformations to build soft machines capable of a programmable sequence of movements with a single actuation input.

Cylindrical shells | Programmable instabilities | Vacuum | Soft structures

Inflatable structures are more than just party balloons; they offer a versatile platform for designing a wide range of lightweight and functional systems, such as temporary shelters (1–4), airbags (5, 6), soft robots (7, 8), and medical devices (9, 10). While load-bearing inflatables are usually made from quasi-inextensible materials, it has been recently shown that the flexibility of stretchable membranes provides new opportunities to realize complex deformations upon inflation (11–14). However, achieving complex deformations often requires intricate initial geometries that pose challenges to fabrication.

Inflatable structures formed from stretchable membranes typically experience tensile stresses. However, it is widely recognized that compressive forces in shells – thin and naturally curved structural components (15, 16) – can trigger mechanical instabilities (17–19). While such instabilities have traditionally been regarded as catastrophic events, one recent trend is that they can be harnessed to design flexible systems with novel functionality (20, 21). This is because in hyper-elastic shells instabilities trigger reversible and repeatable deformations that largely alter the initial geometry and occur over a narrow range of applied load. As such, they have been exploited to realize tunable optical (22) and adhesive (23) properties, encapsulations systems (24), morphable surfaces for aerodynamic drag control (25) and simple machines that can swim (26) or even jump (27).

Here, we demonstrate the potential of exploiting elastic instabilities in thin hyperelastic cylindrical shells to induce complex deformation modes and ultimately build soft machines capable of a programmable sequence of movements using a single input. We first focus on cylindrical shells with homogeneous thickness, which are well-known to buckle upon depressurization. By combining experiments and numerical simulations we reveal a novel insight. Specifically, for shells with a high buckling wave number, we demonstrate that a secondary instability is triggered during the post-buckling regime, suddenly activating a coupled twisting-folding deformation mode. Subsequently, we explore the behavior of cylindrical shells with nonuniform thickness that undergo bending upon depressurization. Much like homogeneous shells, our findings indicate that the deformation of these shells is also instability-driven. Finally, we demonstrate the potential of leveraging the highly nonlinear behavior of elastomeric cylindrical shells to design instability-driven robotic systems capable of executing tasks with minimal actuation input. This is exemplified through the development of a soft manipulator capable of harvesting a cherry tomato with a single input, as well as, grasping an underwater seashell by harnessing the hydrostatic pressure of the environment without the need for an additional external power supply.

Results

Deflation of elastomeric cylindrical shells. We first consider thin-walled cylindrical shells, with inner radius R, thickness t, and height H, that are slowly deflated (Fig. 1A). The critical buckling pressure of these shells, p_{cr}, has been investigated in the context of the failure of cylindrical vessels and analytically determined as (28, 29)

$$\frac{p_{cr}}{E} = \frac{[(\pi R/H)^2 + n^2]^2 (t/R)^3}{12(1-\nu^2)n^2} + \frac{(\pi R/H)^4 (t/R)}{n^2[(\pi R/H)^2 + n^2]^2}, \quad [1]$$

where E and ν denote the Young's modulus and Poisson's ratio of the material, respectively, and n represents the buckling wave number. From Eq. 1, we impose $n \in \{2, 3, \dots\}$ and solve for p_{cr}/E. We then report in Figs. 1B-C the evolution of the lowest p_{cr}/E and its corresponding n for an incompressible material with $\nu = 0.5$. As expected from Eq. 1 and classical works on the stability of shells (30, 31), we find p_{cr}/E increases over several orders of magnitude as t/H increases and R/H decreases, while n increases with R/H and marginally decreases with t/H.

Guided by these results, we consider three cylindrical shells: Shell A with $(t/H,\ R/H) = (0.027, 0.20)$; Shell B with $(t/H,\ R/H) = (0.021, 0.37)$; Shell C with $(t/H,\ R/H) = (0.031, 0.56)$. Note that these three shells are predicted to buckle at $p_{cr}/E = 1.61 \times 10^{-3}$, 3.39×10^{-4}, and 5.32×10^{-4} with $n = 2$, 3, and 4, respectively. We fabricate these three shells by coating rigid cylindrical molds with an elastomer (Zhermack Elite Double 32 with Young's modulus $E = 1.2$ MPa—see Section S1 of the Supplementary Materials for details). In our experiments, we slowly deflate the shells with water using a syringe pump, while monitoring the pressure with a sensor and capturing the deformation via digital cameras (see Section S2 of the Supplementary Materials for details).

Simultaneously, we simulate the nonlinear behavior of the cylindrical shells during deflation by conducting Finite Element (FE) analyses within the commercial package ABAQUS 2019/Standard. We discretize their geometry with 4-node linear shell elements and introduce a geometric imperfection in the form of the first buckling mode. We use an incompressible Neo-Hookean material model with shear modulus $\mu = E/3$ to capture the response of the elastomeric material and simulate the deflation process by running a combination of nonlinear static and implicit dynamic simulations where we slowly decrease the volume of the internal cavity (see Section S3 of the Supplementary Materials for details).

In Figs. 1D-F, we show experimental and FE snapshots of the three shells during deflation. We find good qualitative agreement between experiments and simulations, with all three shells that buckle at first into the theoretically predicted mode. For Shell A, this mode becomes more accentuated upon further deflation, leading to a radial closure. Differently, for Shell B and Shell C the ridges that are formed upon buckling eventually collapse and start twisting leading to pronounced folding. This collapse of the ridges can be attributed to the high axial stresses in these two shells with large R/H (31) (see Section S3E of the Supplementary Materials for details). Note that the coupled twisting/folding deformation mode induced by the collapse of the ridges is reminiscent of that of the Kresling origami module (32), but here is realized in homogeneous shells subjected to deflation by exploiting their nonlinear response.

Next, to better characterize the response of our shells, in Fig. 2A, we report the evolution of their internal pressure p, as a function of the subtracted volume ΔV (normalized by the initial volume of their cavity, V_0), as measured during the tests. Further, in Figs. 2B and 2C, we show the evolution of the axial contraction $\Delta H/H$, and twist angle ϕ, as a function of $\Delta V/V_0$. Note that both $\Delta H/H$ and ϕ are experimentally measured by tracking the position of markers located on

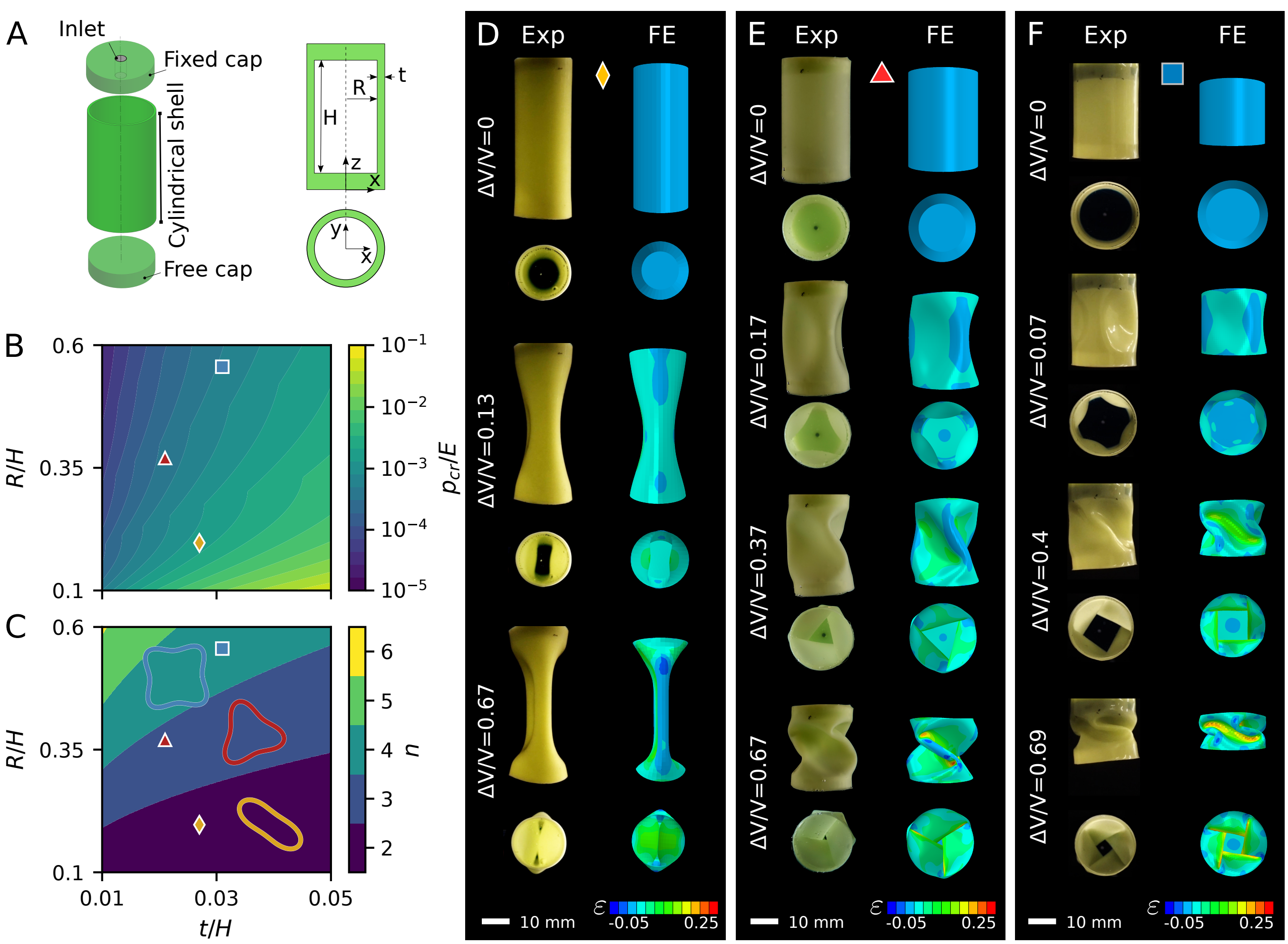

Fig. 1. Vacuum-driven instabilities in thin-walled cylindrical shells. (**A**) Schematics of the system. (**B**)-(**C**) Critical pressure, p_{cr}, and wave number of the first buckling mode, n, as a function of the geometric parameters, t/H and R/H. The markers highlight three cylindrical shell designs: Shell A (diamond) with $(t/H,\ R/H) = (0.027,\ 0.20)$; Shell B (triangle) with $(t/H,\ R/H) = (0.021,\ 0.37)$; Shell C (square) with $(t/H,\ R/H) = (0.031,\ 0.56)$. (**D**)-(**F**) Experimental and Finite Element snapshots of the three shells during deflation at different amounts of subtracted volume, $\Delta V/V_0$. Colorbar shows the maximum in-plane principal strain, ε.

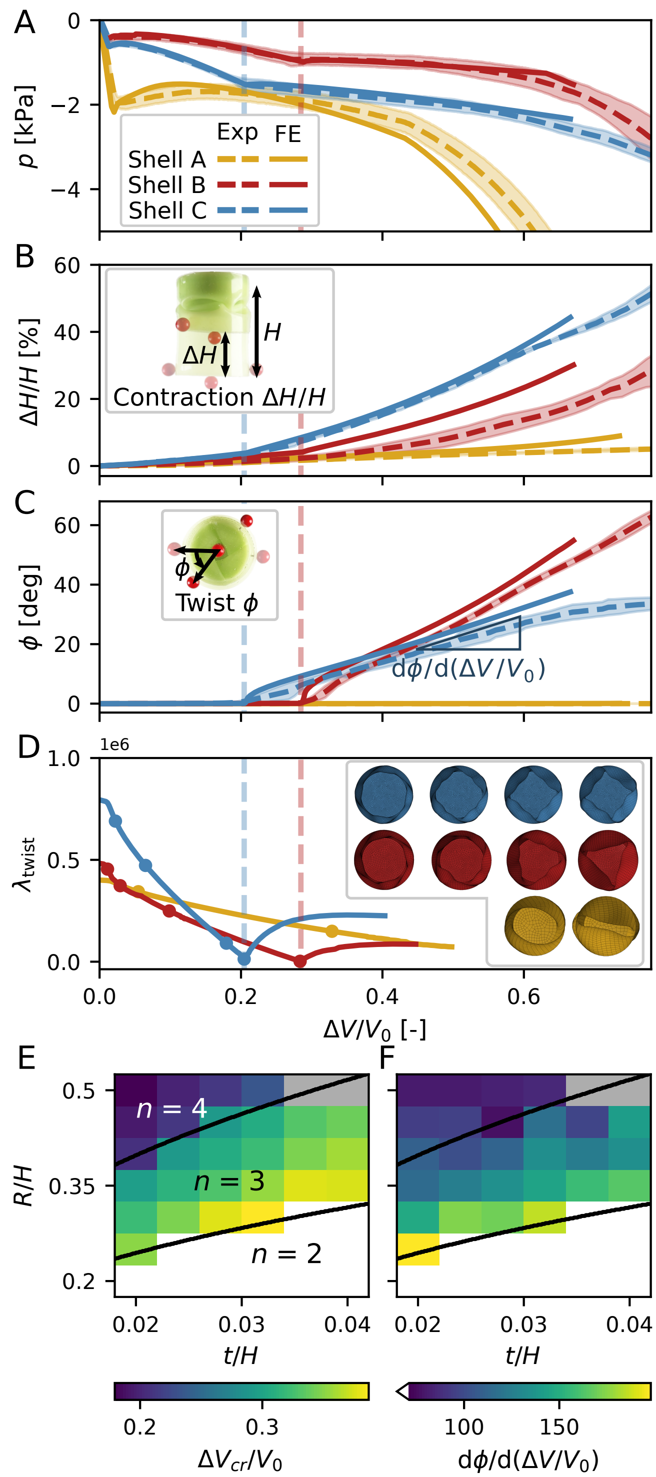

Fig. 2. Post-buckling deformation of cylindrical shells. (**A**)-(**D**) Evolution of (**A**) pressure, (**B**) contraction, (**C**) twist and (**D**) eigenvalue associated to the twisting mode as a function of $\Delta V/V_0$ for Shell A (yellow), Shell B (red) and Shell C (blue). Both experimental (dashed lines with the shaded area representing the standard deviation) and FE results (solid lines) are reported in (**A**)-(**C**). (**E**)-(**F**) Numerically predicted evolution of (**E**) the subtracted volume of fluid at the secondary instability, $\Delta V_{cr}/V_0$, and (**F**) the rate of increase in the twisting deformation after the secondary instability, $\mathrm{d}\phi/\mathrm{d}(\Delta V/V_0)$, as a function of R/H and t/H.

the base of the shells (see insets in Figs. 2B and 2C). Three key features emerge from Figs. 2A-C. First, there is quantitative agreement between experimental and numerical results, confirming the validity of our FE simulations. Second, all pressure-volume curves are characterized by an initial linear regime and a sudden departure from linearity caused by shell buckling. Third, for Shell B and Shell C, an additional sudden change in slope in the pressure-volume curves is found at $\Delta V/V_0 \approx 0.28$ and 0.2, respectively. Remarkably at these values of $\Delta V/V_0$, both $\Delta H/H$ and ϕ suddenly start increasing for Shells B and C, suggesting that an instability is responsible for initiating the prominent twisting/folding deformation mode.

To validate the occurrence of a secondary instability, we conduct additional FE simulations and compute the eigenvalue associated to the twisting/folding mode, λ_{twist}, while gradually reducing the volume within the internal cavity (see Section S3 of the Supplementary Materials for additional details). The results reported in Fig. 2D reveal that for Shell B and Shell C, λ_{twist} attains a local minimum close to zero at $\Delta V/V_0 = 0.285$ and 0.204, respectively. These results confirm that a secondary instability is indeed the governing mechanism behind the twisting/folding deformation mode.

Motivated by these findings, we proceed by simulating the response of shells with $0.02 \leq t/H \leq 0.04$ and $0.2 \leq R/H \leq 0.5$ to identify the region in the design space where the twisting/folding mode is triggered upon deflation. In Figs. 2E and 2F, we report the evolution as a function of the geometry of the subtracted volume of fluid at the secondary instability, $\Delta V_{cr}/V_0$, and the rate of increase in the twisting deformation after the secondary instability, $\mathrm{d}\phi/\mathrm{d}(\Delta V/V_0)$, respectively. We find that shells for which the first buckling mode is characterized by $n = 2$ do not undergo a secondary instability and simply close radially (the white region in the lower right corner of Figs. 2E and 2F). However, shells with $n = 3$ and 4 all exhibit a secondary instability. Within this domain, $\Delta V_{cr}/V_0$ decreases with R/H and increases with t/H, i.e., more volume needs to be subtracted in thick-walled, slender cylindrical shells to trigger twisting. While $\Delta V_{cr}/V_0$ is highly dependent on both t/H and R/H, the geometric effect on $\mathrm{d}\phi/\mathrm{d}(\Delta V/V_0)$ is dominated by R/H—in general, for shells with low R/H values, we find higher rates of increase in the twisting deformation. Additionally, for high values of R/H and t/H (i.e., thick and stocky shells), the secondary instability triggers a shearing-dominated mode rather than a twisting/folding mode (see gray region in Figs. 2E-F and Fig. S16)

Deflation of cylindrical shells with nonuniform thickness. While in Figs. 1 and 2 our focus has been on homogeneous cylindrical shells, we now shift our attention to explore the effects of deflation on shells with nonuniform thickness. Such shells are created by starting with a homogeneous one and reducing the thickness from t to t_r over an angular sector defined by the angle θ (see Fig. 3A and Section S1B of the Supplementary Materials for additional details). In Fig. 3, we consider a shell characterized by $R = 10$ mm, $H = 18$ mm, $t = 0.92$ mm, $t_r = 0.23$ mm and $\theta = 90°$. Due to the difference in stiffness between the two regions with different thicknesses, this inhomogeneous shell bends towards the thinner side upon deflation (see Fig. 3B). Similarly to the homogeneous shells, we see multiple inflection points in the pressure-volume curve

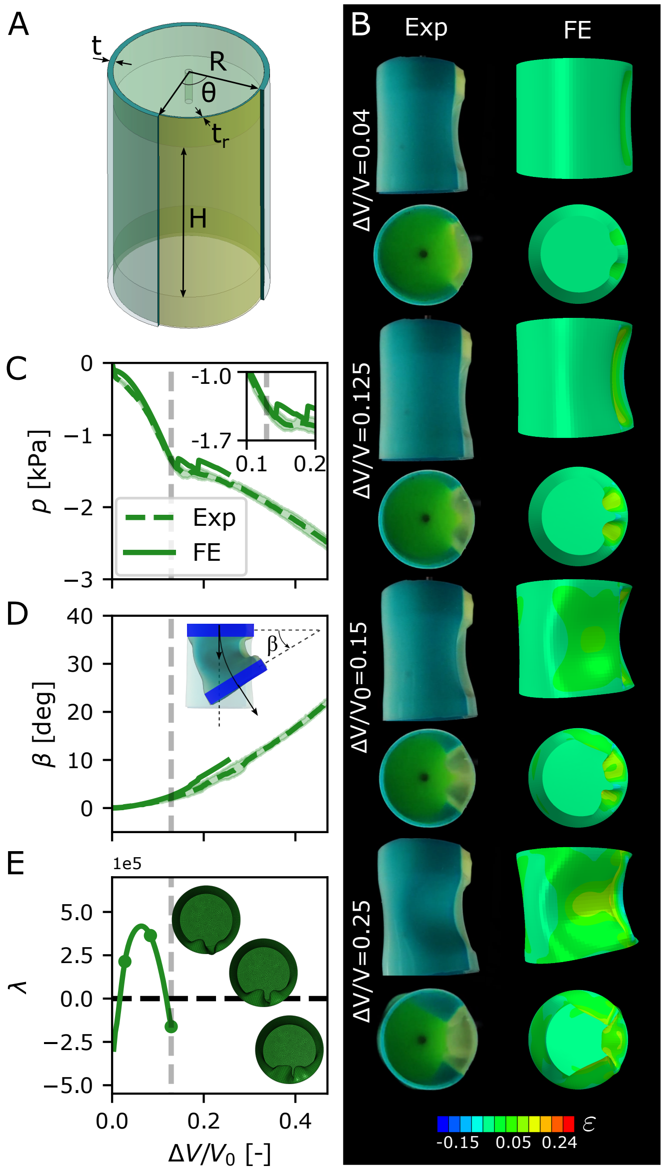

Fig. 3. Bending of cylindrical shells with nonuniform thickness A) Schematics showing a cylindrical shell with reduced thickness t_r (colored with yellow) over an angular sector defined by the angle θ. (**B**) Experimental and Finite Element snapshots during deflation at different amounts of subtracted volume $\Delta V/V_0$. The colorbar shows the maximum in-plane principal strain. (**C**-**E**) Pressure p (**C**), bending angle β (**D**), and eigenvalue λ (**E**) as a function of subtracted volume $\Delta V/V_0$.

(Fig 3C), suggesting that its deformation is once again driven by instabilities. However, in this case, the bending angle β, which is measured between the normal to the free cap and the z-axis, increases smoothly—without a clear onset—with volume removed, reaching approximately 25° for $\Delta V/V_0 = 0.5$ (Fig 3D). Looking closer at the pressure-volume curve, we see two abrupt changes in slope at $\Delta V/V_0 \approx 0.04$ and 0.15. The first change at $\Delta V/V_0 = 0.04$ aligns with the instability predicted by a linear buckling analysis and is associated with the formation of a single inward-pointing ridge in the thinner part of the shell (Fig. 3B). The second abrupt change in slope occurs at $\Delta V/V_0 \approx 0.15$, where the outward pointing ridge in the thin portion of the shell buckles to one side and merges with the ridges formed at the thick-thin boundary (Fig. 3B). Remarkably, our FE analyses reveal the vanishing of an eigenvalue during this event, indicating it as a secondary instability (see Fig. 3E).

Programming sequences in soft systems via instabilities. In general, multimodal deformation in soft elastic systems is achieved either through sophisticated structure designs (33–35), multi-stimuli-responsive polymers (36), stochastic interaction (37), or by introducing multiple actuation inputs (38). Remarkably, the rich post-buckling behavior of cylindrical shells can be exploited to realize sequencing in soft systems actuated by a single pressure input. We illustrate this concept by emulating a human hand grasping a fresh cherry tomato (*Solanum lycopersicum*) on the vine. The robotic system replicates the human harvesting process, made of two distinct steps: (1) the fingers bend to grasp the fruit, and (2) the wrist twists and contracts to disconnect it from the stem (see Fig. 4A).

To realize this bending-twisting-pulling motion, we construct a soft manipulator consisting of three fingers and a wrist (Fig. 4B). Each finger is composed of two bending units—the same geometry as in Fig. 3. These two cylindrical shells are connected in series to amplify the bending angle β induced under vacuum. The wrist is made of a homogeneous cylindrical shell with $(t/H,\ R/H) = (0.033,\ 0.33)$. This geometry is selected from the design map of Fig. 2E to ensure twisting/folding upon depressurization while minimizing the slenderness of the shell (i.e., small height and large thickness) to resist the weight of the cherry tomato. For the successful grasping of a cherry tomato, it is essential for the finger to bend first, followed by the wrist twisting. As illustrated in Fig. 4C, if both the fingers and the wrist are made from the same elastomer, twisting begins before the fingers are fully bent. Therefore, to create a sequence between the deformation of the fingers and the wrist, we fabricate the fingers out of PVS (Zhermack Elite Double 32) with $E = 1.2$ MPa (green dashed line in Fig.4C) and the wrist out of a stiffer silicone elastomer (Smooth-sil 960) with $E = 2.2$ MPa (cyan solid line in Fig. 4C). This design results in a fully soft manipulator capable of replicating the bending-twisting-pulling motion of a human hand. Upon deflation, our gripper generates a maximum torque and pulling force of $T_{\max}^{\text{gripper}} = 2.92$ mN·m±1.24 mN·m and $F_{\max}^{\text{gripper}} = 0.67$ N ± 0.04 N, which is sufficient to successfully unhook the cherry tomato after one to six attempts (see Supplementary Materials, Section S4D for details). Despite our gripper's pressure range and grasping forces being relatively low compared to those reported in the literature (see Supplementary Materials, Table S1), it excels in versatility. Our gripper can execute bending, contraction, and twisting motions when actuated with a single pneumatic input. In addition, $T_{\max}$ and $F_{\max}$ can easily be improved by increasing friction between the fingers and the tomato (see Section S4D of the Supplementary Materials for details).

Discussion and Outlook

In summary, this study focused on the highly nonlinear response of elastomeric cylindrical shells during depressurization. We discovered that in shells with uniform thickness, secondary instabilities initiate complex twisting-folding deformations, which are entirely dictated by their geometry. For shells

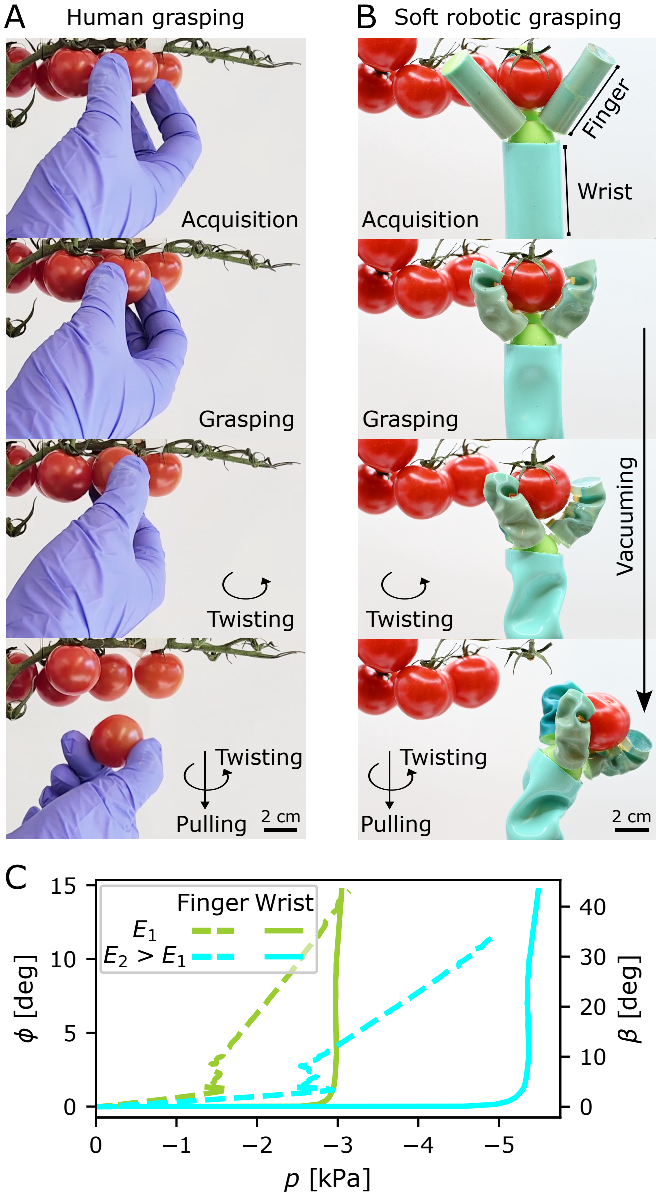

Fig. 4. Instability-driven soft manipulator. (**A**) When harvesting a cherry tomato from a vine, a human hand initially grasps it and then twists it to detach it from the stem. (**B**) This bending-twisting-pulling motion is replicated by a soft manipulator consisting of three fingers and a wrist. (**C**) Bending angle of a finger (dashed lines) and twist angle of the wrist (continuous lines) as a function of pressure for two different elastomers with $E = 1.2$ MPa (green curves) and $E = 2.2$ MPa (cyan curves).

with nonuniform thickness, the deformation is still driven by instabilities, but the uneven flexibility around the circumference leads to pronounced bending. Importantly, when connecting multiple shells in series, we can construct soft systems capable of sequential deformation when actuated with a single input. This was exemplified by the design of a soft manipulator capable of a bending-twisting-pulling motion when actuated by a single pressure source. Integrating these soft machines with innovative control (39) and sensing (40) strategies may lead to the development of soft robots capable of utilizing both fluid and solid mechanics to navigate, sense, and respond to their environment.

While the majority of inflatable actuators typically rely on pressurization for operation, our approach introduces vacuum as the driving force behind shell deformation. One advantage of utilizing vacuum rather than pressure lies in inherent safety, as it mitigates the risk of catastrophic failure due to overpressurization. Moreover, given that hydrostatic pressure in water imposes loading conditions similar to vacuuming in air, our actuators could operate without an external stationary power source in aquatic environments (see Fig. S18).

Materials and Methods

Details of the design, materials, and fabrication methods are summarized in Supplementary Materials, Section S1. The experimental procedure of the inflation with water to measure the pressure-volume curve is described in Supplementary Materials, Section S2. Details on the numerical model can be found in Section S3 of the Supplementary Materials, and additional results are provided in Supplementary Materials, Section S4.

Acknowledgments

Funding: Research was supported by the NSF grants DMR-1922321 and W911NF-22-1-0219. K.B. also acknowledges support from the Simons Collaboration on Extreme Wave Phenomena Based on Symmetries. A.E.F. acknowledges that this project has received funding from the European Unions Horizon 2020 research and innovation program under the Marie Skodowska-Curie grant agreement No 798244. **Author contributions:** Y.Y., D.M., A.E.F., A.Z., and K.B. proposed and developed the research idea. Y.Y. and M.S. designed and fabricated the cylindrical shells. Y.Y. performed experiments. H.R. conducted the numerical simulations. Y.Y., H.R., D.M., and K.B. wrote the paper. D.M. and K.B. supervised the research. **Competing interests:** The authors declare no conflict of interest. **Data and materials availability:** The data that support the findings of this study are openly available in github at https://github.com/bertoldi-collab/buckling-cylinders.

References

1. Monty Fritts and Darren J Myers. Inflatable shelter, April 16 1991. US Patent 5,007,212.
2. Robert T Kendall Jr. Inflatable emergency shelter, May 20 1997. US Patent 5,630,296.
3. Eric J McNiff, Christopher G Rowen, and Paul Calabro. Inflatable tent, November 23 1999. US Patent 5,987,822.
4. D. Melancon, B. Gorissen, C. J. García-Mora, C. Hoberman, and K. Bertoldi. Multistable inflatable origami structures at the metre scale. *Nature*, 592:545–550, 2021.
5. John W Hetrick. Safety cushion assembly for automotive vehicles, August 18 1953. US Patent 2,649,311.
6. Janine Jagger, Katherine Vernberg, and John A Jane. Air bags: reducing the toll of brain trauma. *Neurosurgery*, 20(5):815–817, 1987.
7. Daniela Rus and Michael T. Tolley. Design, fabrication and control of soft robots. *Nature*, 521 (7553):467–475, May 2015. ISSN 1476-4687. . URL https://doi.org/10.1038/nature14543.
8. Carmel Majidi. Soft robotics: A perspective—current trends and prospects for the future. *Soft Robotics*, 1(1):5–11, Mar 2014. ISSN 2169-5172. . URL https://doi.org/10.1089/soro.2013.0001.
9. Jacob Rogatinsky, Dominic Recco, Joseph Feichtmeier, Yuchen Kang, Nicholas Kneier, Peter Hammer, Edward OLeary, Douglas Mah, David Hoganson, Nikolay V. Vasilyev, and Tommaso Ranzani. A multifunctional soft robot for cardiac interventions. *Science Advances*, 9(43): eadi5559, 2023. . URL https://www.science.org/doi/abs/10.1126/sciadv.adi5559.
10. Ellen T. Roche, Markus A. Horvath, Isaac Wamala, Ali Alazmani, Sang-Eun Song, William Whyte, Zurab Machaidze, Christopher J. Payne, James C. Weaver, Gregory Fishbein, Joseph Kuebler, Nikolay V. Vasilyev, David J. Mooney, Frank A. Pigula, and Conor J. Walsh. Soft robotic sleeve supports heart function. *Science Translational Medicine*, 9(373):eaaf3925, Jan 2017. . URL https://doi.org/10.1126/scitranslmed.aaf3925.
11. Tian Gao, José Bico, and Benoît Roman. Pneumatic cells toward absolute gaussian morphing. *Science*, 381(6660):862–867, 2023. . URL https://www.science.org/doi/abs/10.1126/science.adi2997.
12. Antonio Elia Forte, Paul Z. Hanakata, Lishuai Jin, Emilia Zari, Ahmad Zareei, Matheus C. Fernandes, Laura Sumner, Jonathan Alvarez, and Katia Bertoldi. Inverse design of inflatable soft membranes through machine learning. *Advanced Functional Materials*, 32(16):2111610, 2022. . URL https://onlinelibrary.wiley.com/doi/abs/10.1002/adfm.202111610.
13. Robert Baines, Sree Kalyan Patiballa, Benjamin Gorissen, Katia Bertoldi, and Rebecca KramerBottiglio. Programming 3D Curves with Discretely Constrained Cylindrical Inflatables. *Advanced Materials*, 35(26):2300535, June 2023. ISSN 0935-9648, 1521-4095. . URL https://onlinelibrary.wiley.com/doi/10.1002/adma.202300535.
14. Trevor J. Jones, Etienne Jambon-Puillet, Joel Marthelot, and P.-T. Brun. Bubble casting soft robotics. *Nature*, 599(7884):229–233, Nov 2021. ISSN 1476-4687. . URL https://doi.org/10.1038/s41586-021-04029-6.

15. Basile Audoly and Yves Pomeau. Elasticity and geometry. 2000.
16. Stephen Timoshenko, Sergius Woinowsky-Krieger, et al. *Theory of plates and shells*, volume 2. McGraw-hill New York, 1959.
17. Dominic Vella. Buffering by buckling as a route for elastic deformation. *NATURE REVIEWS PHYSICS*, 1(7):425–436, JUL 2019. .
18. Anna Lee, Francisco López Jiménez, Joel Marthelot, John W Hutchinson, and Pedro M Reis. The geometric role of precisely engineered imperfections on the critical buckling load of spherical elastic shells. *Journal of Applied Mechanics*, 83(11):111005, 2016.
19. John W Hutchinson. Buckling of spherical shells revisited. *Proceedings of the Royal Society A: Mathematical, Physical and Engineering Sciences*, 472(2195):20160577, 2016.
20. Pedro M. Reis. A Perspective on the Revival of Structural (In)Stability With Novel Opportunities for Function: From Buckliphobia to Buckliphilia. *Journal of Applied Mechanics*, 82(11), 09 2015. ISSN 0021-8936. . URL https://doi.org/10.1115/1.4031456.
21. Douglas P. Holmes. Elasticity and stability of shape-shifting structures. *Current Opinion in Colloid & Interface Science*, 40:118–137, 2019. ISSN 1359-0294. . URL https://www.sciencedirect.com/science/article/pii/S1359029418300839. Particle Systems.
22. D.P. Holmes and A.J. Crosby. Snapping surfaces. *Advanced Materials*, 19(21):3589–3593, 2007.
23. Guangchao Wan, Yanbing Tang, Kevin T. Turner, Teng Zhang, and Wanliang Shan. Tunable dry adhesion of soft hollow pillars through sidewall buckling under low pressure. *Advanced Functional Materials*, 33(2):2209905, 2023. . URL https://onlinelibrary.wiley.com/doi/abs/10.1002/adfm.202209905.
24. Jongmin Shim, Claude Perdigou, Elizabeth R. Chen, Katia Bertoldi, and Pedro M. Reis. Buckling-induced encapsulation of structured elastic shells under pressure. *Proceedings of the National Academy of Sciences*, 109(16):5978–5983, 2012. . URL https://www.pnas.org/doi/abs/10.1073/pnas.1115674109.
25. Denis Terwagne, Miha Brojan, and Pedro M. Reis. Smart morphable surfaces for aerodynamic drag control. *Advanced Materials*, 26(38):6608–6611, 2014. . URL https://onlinelibrary.wiley.com/doi/abs/10.1002/adma.201401403.
26. Adel Djellouli, Philippe Marmottant, Henda Djeridi, Catherine Quilliet, and Gwennou Coupier. Buckling instability causes inertial thrust for spherical swimmers at all scales. *Phys. Rev. Lett.*, 119:224501, Nov 2017. . URL https://link.aps.org/doi/10.1103/PhysRevLett.119.224501.
27. Benjamin Gorissen, David Melancon, Nikolaos Vasios, Mehdi Torbati, and Katia Bertoldi. Inflatable soft jumper inspired by shell snapping. *Science Robotics*, 5(42):eabb1967, 2020. . URL https://www.science.org/doi/abs/10.1126/scirobotics.abb1967.
28. Windenburg Dwigh and Charles Trilling. Collapse by instability of thin cylindrical shells under external pressure. *Trans. ASME*, 56(8):819–825, 1934.
29. Don O. Brush and Bo O. Almroth. *Buckling of Bars, Plates, and Shells*. McGraw-Hill Engineering, New York, 1975.
30. Dwight F. Windenburg and Charles Trilling. Collapse by Instability of Thin Cylindrical Shells Under External Pressure. *Journal of Fluids Engineering*, 56(8):819–825, August 1934. ISSN 0097-6822. . URL https://asmedigitalcollection.asme.org/fluidsengineering/article/56/8/819/1157766/Collapse-by-Instability-of-Thin-Cylindrical-Shells.
31. S. B. Batdorf. A simplified method of elastic-stability analysis for thin cylindrical shells 1: Donnell's equation. Report, University of North Texas Libraries, UNT Digital Library, June 1947. URL https://digital.library.unt.edu/ark:/67531/metadc54406/. Accessed: July 16, 2024.
32. Biruta Kresling. Origami-structures in nature: lessons in designing smart materials. *MRS Proceedings*, 1420:mrsf11–1420–oo02–01, 2012. ISSN 0272-9172, 1946-4274. . URL http://link.springer.com/10.1557/opl.2012.536.
33. Chao Zhang, Zhuang Zhang, Yun Peng, Yanlin Zhang, Siqi An, Yunjie Wang, Zirui Zhai, Yan Xu, and Hanqing Jiang. Plug & play origami modules with all-purpose deformation modes. *Nature Communications*, 14(1):4329, Jul 2023. ISSN 2041-1723. . URL https://doi.org/10.1038/s41467-023-39980-7.
34. Shuai Wu, Qiji Ze, Jize Dai, Nupur Udipi, Glaucio H. Paulino, and Ruike Zhao. Stretchable origami robotic arm with omnidirectional bending and twisting. *Proceedings of the National Academy of Sciences*, 118(36):e2110023118, 2021. . URL https://www.pnas.org/doi/abs/10.1073/pnas.2110023118.
35. Arnaud Lazarus and Pedro M. Reis. Soft actuation of structured cylinders through auxetic behavior. *Advanced Engineering Materials*, 17(6):815–820, 2015. . URL https://onlinelibrary.wiley.com/doi/abs/10.1002/adem.201400433.
36. Qiguang He, Zhijian Wang, Yang Wang, Adriane Minori, Michael T. Tolley, and Shengqiang Cai. Electrically controlled liquid crystal elastomerbased soft tubular actuator with multimodal actuation. *Science Advances*, 5(10):eaax5746, October 2019. ISSN 2375-2548. . URL https://www.science.org/doi/10.1126/sciadv.aax5746.
37. Kaitlyn Becker, Clark Teeple, Nicholas Charles, Yeonsu Jung, Daniel Baum, James C. Weaver, L. Mahadevan, and Robert Wood. Active entanglement enables stochastic, topological grasping. *Proceedings of the National Academy of Sciences*, 119(42):e2209819119, October 2022. ISSN 0027-8424, 1091-6490. . URL https://pnas.org/doi/10.1073/pnas.2209819119.
38. Qiguang He, Zhijian Wang, Yang Wang, Adriane Minori, Michael T. Tolley, and Shengqiang Cai. Electrically controlled liquid crystal elastomerbased soft tubular actuator with multimodal actuation. *Science Advances*, 5(10):eaax5746, 2019. . URL https://www.science.org/doi/abs/10.1126/sciadv.aax5746.
39. Bert Van Raemdonck, Edoardo Milana, Michael De Volder, Dominiek Reynaerts, and Benjamin Gorissen. Nonlinear Inflatable Actuators for Distributed Control in Soft Robots. *Advanced Materials*, 35(35):2301487, September 2023. ISSN 0935-9648, 1521-4095. . URL https://onlinelibrary.wiley.com/doi/10.1002/adma.202301487.
40. Shibo Zou, Sergio Picella, Jelle de Vries, Vera G. Kortman, Aimée Sakes, and Johannes T. B. Overvelde. A retrofit sensing strategy for soft fluidic robots. *Nature Communications*, 15(1):539, January 2024. ISSN 2041-1723. . URL https://www.nature.com/articles/s41467-023-44517-z.